中國機械工程學刊第四十三卷第六期第 549~558 頁(民國一百一十一年)
Journal of the Chinese Society of Mechanical Engineers, Vol.43, No.5, pp.549~558(2022)

Effect of Serrated Endmill Geometry on Machining Responses of Al 2024 Thin-Walled Components

Darshan S**, Shivaraj BW *, Bharatish A*, Krishna M***, Narasimha Murthy HN***

Keywords：Serrated End mills, Thin wall Deflection, Helix angle, Machining, Al 2024

ABSTRACT

Thin-walled components are widely adopted in aircraft structures due to the eminent characteristics such as light weight, high strength to weight ratio, high usability and ergonomics. However, the lower stiffness of these components results in static and dynamic instabilities during their machining. Thus, there is a requirement to reduce the deflection, stresses and unwanted vibrations during machining of thin-walled components. Adoption of serrated end mill can cause non-uniform distribution of chip thickness, reduction of effective axial depth of cut and cutting forces and improvement of chatter stability. This paper focuses on investigating the effect of serrated end mill geometrical parameters such as the number of flutes (2, 3, and 4), helix angle (30º, 35º, and 45º) and serration geometry (sinusoidal, median, and interrupted) on machining responses of thin-walled components. The deflections and stresses were computed using ANSYS explicit dynamics module. The thin wall deflection was mainly influenced by number of flutes and stresses by helix angle. The machining responses could be simultaneously minimized when maximum number of flutes, intermediate helix angle and median serration geometry were adopted.

INTRODUCTION

Thin-walled components are widely used in aircraft structures due to their eminent properties such as low weight, high strength to weight ratio and contribution to aircraft fuel efficiency.

Machining of these components is the major challenge faced during aircraft manufacturing due to productivity issues, static and dynamic instabilities of the thin wall during machining. These parts are manufactured by removing a bulk amount of material from the stock by achieving a 30:1 buy to fly ratio (Herranz et al., 2005). Typically, 90-95 % of material is removed from the monolithic block to arrive at the required thin-walled component (Kersting and Biermann, 2014), which leads to consumption of high amount of production time and also an increase in the cutting tool cost due to high tool wear. Thin-walled parts generally have lower stiffness which results in static and dynamic problems during their machining. The clamping forces due to work holding and cutting forces induced by cutting tools produce elastic deformation during machining, which can affect the final dimensionality and the surface roughness of the machined part (Chen et al., 2009; Rai and Xirouchakis, 2009). The residual stresses induced during machining also adversely affects the final geometry of the machined part (Jiang et al., 2018). Serrated endmills are cutter tools used in milling operation with serrations along the periphery of its cutting edges. A standard serrated endmill is as shown in Fig. 1. These types of endmills are used in the applications which requires low cutting forces, chatter free operation, superior chip breaking and high Material removal rate (Guo et al., 2019). Due to the serration, the diameter of the serrated endmill continuously changes along its axis whereas the diameter of the conventional endmill is constant throughout its length (Bari et al., 2019). The serration parameters such as serration profile and phase shift lead to the variation in local rake and oblique angles, which affects the mechanics and dynamics of machining. The serrations along the length of the cutting-edge results in non-uniform distribution of chip thickness, which results in a decrease of effective axial depth of cut, thus reducing the cutting forces and improving chatter stability (Jiang et al., 2013).

Paper Received July, 2022. Revised September, 2022. Accepted October, 2022. Author for Correspondence: Shivaraj BW.

** Assistant Professor, Department of Mechanical Engineering, RV College of Engineering, Bengaluru, 560059, India*

*** Graduate Student, Department of Mechanical Engineering, RV College of Engineering, Bengaluru, 560059, India.*

****Professor, Department of Mechanical Engineering, RV College of Engineering, Bengaluru, 560059, India*

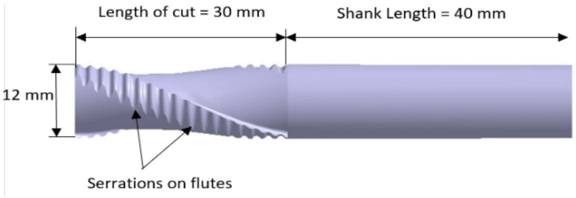

Fig. 1. Serrated Endmill

The effects of tool geometry (Izamshah et al., 2013) tool path strategies (Wan et al., 2011) and the machining parameters (li et al., 2019) on the thin wall properties such as deformation, surface texture, residual stress were reported by many of the researchers. (Wan et al., 2011) proposed a thin wall deflection prediction and tool path adjustment model to reduce the machining error that are caused due to deflection of thin wall during machining. The experimental results showed that the tool path adjustment can avoid the problems such as undercutting and over cutting that leads to thin wall deflection and also reduce the geometric errors such as dimension error, profile error and parallelism error in the machined thin-walled part. (Junbai et al., 2011) applied multipoint location theory for manufacturing large scale thin wall workpiece using flexible tooling system. They reported a decrease in the machining error and manufacturing cycle time, when flexible tooling system coupled with the multi-point location/support algorithm was used for thin wall machining. (Zeng et al., 2012) proposed a new fixture design method to reduce the vibrations in the flexible structural components during machining. They observed that the proposed method could effectively predict the vibrational characteristics of the workpiece being machined and also reduce the profile errors such as surface waviness on the machined region.

Joshi et al. (2017) performed numerical simulations on machining of thin-walled Al 2024 components to predict the product quality in terms of deflection and section thickening during machining. The authors reported that the simulation results (thin wall deflection) were in good agreement with the experimental results with maximum percentage error of 20.17 %. (Wu et al., 2020) developed a new predictive model to analyze the effect of cutting load on the part deformation during milling of thin-walled parts. The model included the effects of tool wear and temperature developed in the tool-workpiece contact region based on oblique cutting analysis. They concluded that prediction of thin wall deformation in the presence of tool wear and proper choice of cutting parameters play an important role to avoid chatter damage and improve the surface quality of the machined surface. (Gang, 2009) performed FEA simulation and experimental analysis of milling of a thin-walled workpiece with a cantilever plate structure using a helical fluted end mill. The simulated model was in a reasonable agreement with the experimental results with percentage error of 21.56 % between the simulation and experimental results. (Aijun et al., 2008) developed an analytical model to study the deformations of thin-walled plates caused by end milling forces, where the deformations were predicted using reciprocal theorem. The simulation results showed that linear loads, milling cutter location and thickness of the thin wall plate have a significant influence on thin wall deflection.

To predict the cutting forces observed in the milling process using serration endmills, some of the researchers have proposed cutting force models (Dombovari et al., 2010; Tehranizadeh et al. 2019). (Koca and Budak, 2013) investigated the effect of tool geometry on the mechanics and dynamics of the serration endmills by developing a milling force model. The developed model was used to optimize the serrated endmills to lower the milling forces. The experimental investigation showed 10 % decrease in cutting forces when compared to commercially available serrated endmills. (Bari et al., 2019) developed a geometric force model (GFM) to study the effects of serration geometry parameters on cutting force during milling operations using serrated end mill cutters. The developed force model was experimentally validated and it was further subjected to sensitivity analysis to evaluate the effects of serration parameters between successive teeth on cutting force. There results showed that cutting force is very sensitive to the change in serration wavelength, serration phase shift and less sensitive to the change in serration amplitude.

Burek et al. (2019) performed experimental studies on the High-performance milling of AlZn5.5MgCu aluminum alloy using end mill cutters incorporating continuous, interrupted and wavy serration geometry. They reported the reduction in the cutting force by up to 35 % in feed direction, 25 % in normal to feed direction and 18 % in axial direction cutting force components. And also showed the cutting force components independency from depth of cut for the optimized serrated endmill, suggesting increased milling efficiency that can be achieved using higher depth of cut compared to convention endmills, without affecting the tool life. (Okafor and Sultan et.al., 2016) developed a mechanistic cutting force prediction model for the wavy-edge, bull-nose, helical endmill (WEBNHE) in order to investigate the effects of the geometrical parameters on the cutting force components and their resultant during high-speed end-milling of Inconel 718. The experimental analysis showed that the cutting force components were in good agreement both in magnitude and trend with the simulated results and lower cutting forces were observed when the WEBNHE was used at higher spindle speed of 92 rpm.

From the review of literatures, it was found that researchers have mainly focused on improving the quality and productivity of machining of thin wall components using standard helical end mills. Also, the end milling process was simulated by considering the various parameters such as cutting speed, feed rate, and depth of cut and so on. The adoption of serrated endmill in the applications which requires low cutting forces imposes challenges in terms of chatter free operation, superior chip breaking and achieving higher material removal rate. Machining of thin-walled aircraft components imposes technical challenges such as large deformations due to low rigidity of workpiece and surface errors due to chatter phenomenon during machining. Hence, the research pertaining to the simulation of machining of these thin-walled components using serration profile endmills assumes utmost importance and needs to be explored yet. The present research focusses on investigating the effect of geometrical parameters such as number of flutes, helix angle and serration geometry on the quality of Al 2024 machined component measured in terms of thin wall deflection and stress distribution. The numerical simulation was performed using ANSYS Explicit Dynamics V 18.1 finite element analysis package. Simulation runs were designed based on L9 orthogonal array. The significant factors were identified through ANOVA and multi objective optimization was carried out based on Grey Relational Analysis (GRA). The optimal solution was also confirmed through simulation runs.

SIMULATION OF MILLING OF AL 2024 THIN WALL PART USING SERRATED ENDMILL

The milling simulation of aluminum alloy 2024 thin-walled part, machined using serrated endmill was performed using ANSYS Explicit Dynamics. The geometrical parameters considered were the number of flutes, helix angle and serration geometry profile of endmills. The factors and their respective levels are as shown in the Table 1.

Table 1. Serrated endmill geometric parameters and their levels

	Factors	Level 1	Level 2	Level 3
1	Number of flutes	2	3	4
2	Helix angle	30^0	35^0	45^0
3	Serration Geometry	Sinusoidal	Median	Interrupted

The simulation layout for performing the numerical analysis of machining of a thin-walled part using serrated endmill based on Taguchi L9 orthogonal array is as shown in Table 2.

Table 2. Simulation layout using L9 OA to perform numerical simulation

Run No.	Parameters		
	No of Flutes	Helix angle	Serration Geometry
1	2	30^0	Sinusoidal
2	2	35^0	Median
3	2	45^0	Interrupted
4	3	30^0	Median
5	3	35^0	Interrupted
6	3	45^0	Sinusoidal
7	4	30^0	Interrupted
8	4	35^0	Sinusoidal
9	4	45^0	Median

Geometry of the thin-walled workpiece and serrated endmill

The cutting tool used for performing the thin wall machining was a helical end mill cutters with serrations along its flutes. The endmill diameter of 12 mm, overall length 70 mm and length of cut of 30 mm were considered for the modeling of tools. The three-dimensional geometric models of serrated endmills and thin-walled work pieces were created using CATIA V5 software. The required dimensions of the thin-walled workpiece used for modelling were considered from (Joshi et al 2017). The thickness for the thin wall was maintained at 5 mm. The assembly of thin-walled work piece and serrated end mill is as shown in the Fig. 2. The sinusoidal, median and interrupted serration geometrical profiles are as shown in Fig. 3(a) – (c).

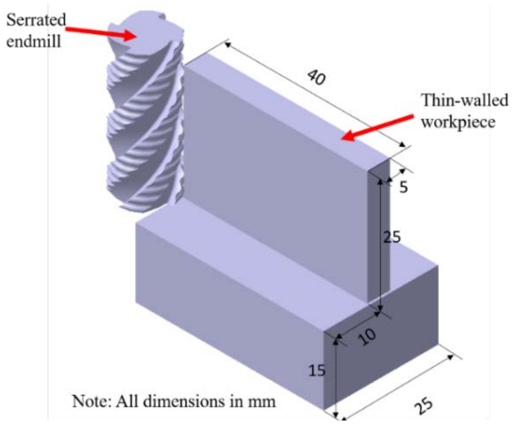

Fig. 2. Thin-walled workpiece and serrated endmill assembly

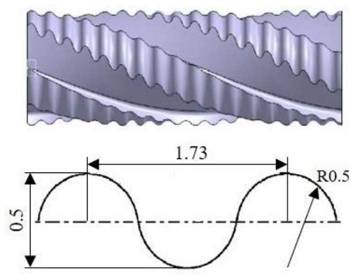

(a) Sinusoidal

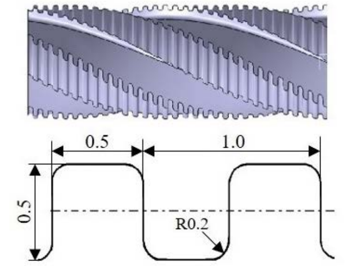

(b) Median

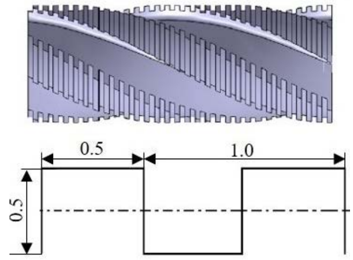

(c) Interrupted

Fig. 2 (a) – (c) Serration geometrical profiles

Material properties and Dynamic failure model

The serrated cutters were assigned Tungsten Carbide (WC) material and the thin-walled workpiece was assigned aluminium alloy 2024 material to perform the numerical simulation. Johnson-cook constitutive equation was used to describe the plastic behavior of the aluminium alloy material in simulating the chip flow during the milling process. The flow stress or effective stress considering the effects of strain hardening, strain rate hardening and thermal softening was described as given by Equation (1) (Li et al., 2021). The parameters of Johnson-cook constitutive equation for the Aluminium alloy 2024 material used in the simulation (Joshi et al 2017) are as given in Table 3.

$$\bar{\sigma} = (A + B\bar{\varepsilon}^n)\left[1 + C\ln\left(\frac{\dot{\bar{\varepsilon}}}{\dot{\bar{\varepsilon}}_0}\right)\right]\left[1 - \left(\frac{T-T_r}{T_m-T_r}\right)^m\right] \qquad (1)$$

Where $\bar{\sigma}$ is the flow stress, A is initial yield stress, B hardening constant, C strain rate constant, n hardening exponent and m is thermal softening exponent. $\bar{\varepsilon}$ is the effective plastic strain, $\dot{\bar{\varepsilon}}$ is the effective plastic strain rate and $\dot{\bar{\varepsilon}}_0$ is the reference effective plastic strain. T is the instantaneous temperature of workpiece, T_r is the room temperature and T_m is the melting temperature of the workpiece.

Table 3. Johnson and Cook material coefficients for AL 2024-T351

Parameter	A (MPa)	B (MPa)	C	N	M
Value	352	440	0.0083	0.42	1

Johnson-cook dynamic failure model was used in conjunction to Johnson-cook plasticity model to specify the damage initiation and evolution that govern the degradation and removal of the elements from a given mesh. Table 4 shows the values of the Johnson-cook failure parameters of the alloy 2024 material used in the simulation, where D represents the damage constants (Joshi et al. 2017). According to (Masmali and Mathew, 2017), the amplitude of displacement and cutting forces induced in the workpiece in normal direction during up milling process was less than those induced during down milling process. Thus, vibration levels of end mills could be reduced by adopting the up milling process. Thus, the finite element model of up milling process was adopted.

Table 4. Johnson–Cook failure parameters for AL 2024-T351

Parameter	D1	D2	D3	D4	D5
Value	0.13	0.13	-1.5	0.011	0

Meshing and boundary conditions

The stiffness of the cutting tool was defined as ‘Rigid’, whereas workpiece stiffness behaviour was defined as ‘Flexible’, as tool deflection during machining was negligible compared to the workpiece deflection. The contact between the cutter tool and the workpiece is important to be specified because it defines the chip formation process during the milling operation. The contact type between the cutting tool and the workpiece was defined using modified coulombs friction law. The friction coefficient between the cutter tool and the workpiece was assigned as 0.17. For meshing the workpiece geometry, hexahedral elements were used throughout the body to balance the accuracy of the simulation and computation time of the solution. The Higher mesh density with element size of 0.35 mm was used near workpiece area which was to be machined. For meshing the cutter tool geometry, tetrahedral elements were used throughout the body. The flutes of the serrated endmills were finely meshed with the element size of 0.5 mm and the other regions of the tool were coarsely meshed.

The boundary conditions used for the simulation is as shown in the Fig. 4.

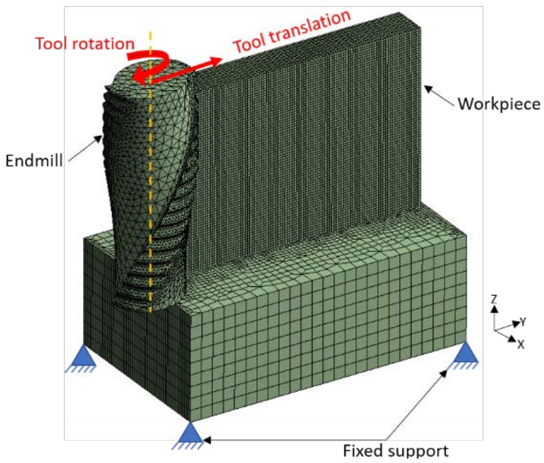

Fig. 4. Tool workpiece meshing and boundary conditions

The thin-walled component was fixed at the bottom face of the part (Ux=Uy=Uz=0), thus restricting all of the degrees of freedoms in that face. The cutting tool was provided with the translatory (Uy=47mm, Ux=0 and Uz=0) as well as rotary motion (θz=-2600°, θx=0°, θy=0°) according to the machining parameters specified in Table 5.

Table 5. Machining parameters considered for simulation

Parameter	Value	Units
Radial depth of cut	1	mm
Axial depth of cut	23	mm
Spindle speed	6000	RPM
Feed rate	11.75	mm/s
Milling type	Up milling	

RESULTS AND DISCUSSIONS

Effect of endmill geometrical parameters on thin wall deflection

The thin wall deflection and stress distribution results obtained from each simulation is presented in the Table 6. The deflection at the free end of the thin-walled part was measured, since thin wall section is analogous to a cantilever system, for which maximum deflection occurs at the free end. The maximum and minimum deflection of 1.032 mm and 0.72 mm was observed in the thin-walled part corresponding to 2 flutes, 30^0 helix angle, sinusoidal serration geometry endmill (Run no 1) and 4 flutes, 45^0 helix angle, median serration endmill (Run no 9) respectively.

Table 6. Response table for thin wall deflection and stresses

Run No.	Parameters			Responses	
	No of Flutes	Helix angle	Serration Geometry	Deflection (mm)	Stress distribution (MPa)
1	2	30^0	Sinusoidal	1.032	544.16
2	2	35^0	Median	0.955	487.76
3	2	45^0	Interrupted	0.831	517.5
4	3	30^0	Median	0.816	538.16
5	3	35^0	Interrupted	0.835	505.72
6	3	45^0	Sinusoidal	0.859	542.36
7	4	30^0	Interrupted	0.77	561.56
8	4	35^0	Sinusoidal	0.812	541.38
9	4	45^0	Median	0.72	541.63

The maximum and minimum deflections observed in the thin-walled component is as shown in the Fig. 5(a) – (b). As the thin wall deflection increases, the un-machined area also increases leading to undesired surface errors. Also, the thickness is lower at the bottom and gradually increases towards the top in the machined area which is a form of surface error caused due to wall deflection.

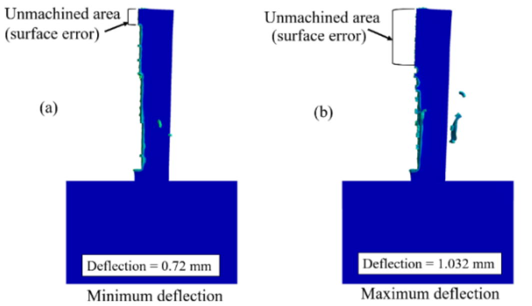

Fig. 5(a) – (b). Thin wall deflection results

Fig. 6 shows the thin wall deflection at discrete points measured along the tool feed direction at top, middle and bottom portions of the thin wall. This deflection corresponds to 4 flute, 45^0 helix angle, median serration geometry (Run no-9) and the trend remains similar for other conditions also. The maximum deflection was observed at the start and end of the thin wall because the thin wall is more rigid at the center than at the edges hence deflect more at the free ends due to the action of the cutting forces (Izamshah et al., 2013); (Li et al., 2019).

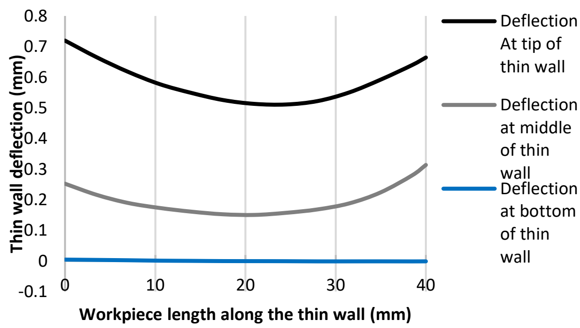

Fig. 6. Thin wall deflections along the length of the workpiece

Fig. 7 shows the main effects plot for deflection of thin-walled component. As the number of flutes increases, the thin wall deflection decreases. The increase in the number of flutes leads to a decrease in engagement time between the cutting tooth and the workpiece. This in turn leads to a decrease in cutting forces induced on the workpiece due to a decrease in the chip load (Li et al., 2021). This reduction in the cutting forces leads to a decrease in the workpiece deflection. As the helix angle increases, the thin wall deflection decreases. As the helix angle of end mill decreases, the cutting force increases which cause higher workpiece deflection due to chatter and reduction in tool-workpiece engagement time. Hence an increase in helix angle leads to a decrease in thin wall deflection (Izamshah et al., 2013). Maximum thin wall deflection was observed for sinusoidal serrated endmill and minimum deflection for interrupted serrated geometry end mill. The variation in the cutting forces becomes minimum with change in tool rotation angle for Interrupted serration geometry when compared to that of sinusoidal or circular geometry. This results in reduction of workpiece deflection (Tehranizadeh and Budak, 2017). However, the number of flutes was the most influential factor effecting the thin wall deflection (Naveed Iqbal Ansari et al., 2021).

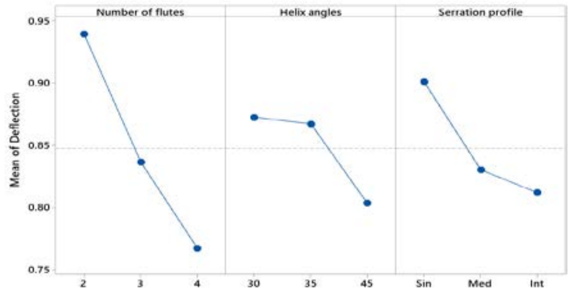

Fig. 7. Main effects plot for thin wall deflection

ANOVA for thin wall deflection

ANOVA was carried out to determine the significance and percentage of the contribution of each factor towards the thin wall deflection. Table 7 shows the results of ANOVA obtained for the thin wall deflection.

Table 7. ANOVA for thin wall deflection

Factor	DoF	Seq SS	Contribution(%)	Adj MS	p-value	F_{cal}	$F_{0.05}$
Number of flutes	2	0.040982	66.19	0.020491	0.034	28.36	19
Helix angles	2	0.008738	14.11	0.004369	0.142	6.03	19
Serration geometry	2	0.010743	17.35	0.005372	0.119	7.41	19
Error	2	0.00145	2.34	0.000725			
Total	8	0.061913	100				

The Number of flutes parameter had the largest percentage contribution of 66.2 % followed by Serration profile at 17.35 % and Helix angles at 14.1 %. Since F_{cal} value for the number of flutes parameter was greater than the critical F-value ($F_{0.05, 2, 2}$) with 95 % confidence level, the number of flutes was the most significant parameter in this case.

Effect of endmill geometrical parameters on stress distribution in the thin wall

Table 6 shows the maximum stress in the thin wall obtained from the simulation. The maximum and minimum stresses of 561.56 MPa and 487.76 MPa observed in the thin-walled part corresponded to 4 flutes, 30^0 helix angle, interrupted serration geometry endmill (Run no 7) and 2 flutes, 35^0 helix angle, median serration endmill (Run no 2) respectively and is as shown in the Fig. 8. The maximum stresses in the machined region were greater than the material yield strength because of plastic deformation in the region causing metal removal.

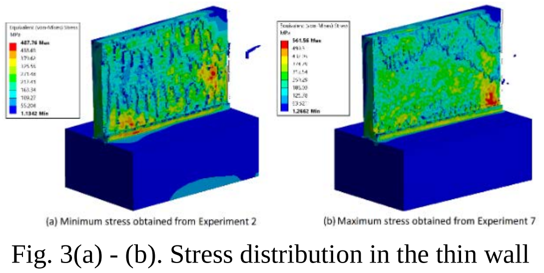

Fig. 3(a) - (b). Stress distribution in the thin wall

Fig. 9 shows the variation of von misses stress in the machined region of thin wall during the milling operation for simulation Run no 2 (2 flutes, 30º helix angle, and median serration geometry) and the trend remains similar for other conditions also.

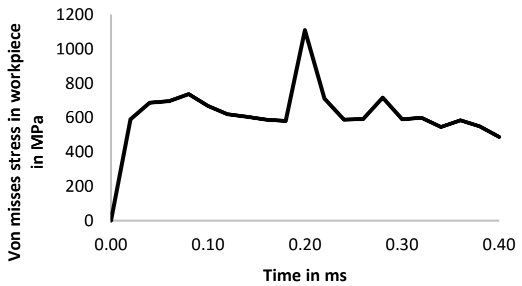

Fig. 9. Stress variation in the thin-walled workpiece during machining

It can be observed that at the start of machining, before the tool interacts with the workpiece, the stress is zero. As the machining begins and the cutter tool starts removing the workpiece material in the form of chips, the stresses in the workpiece increases and reaches maximum at the middle of the workpiece where workpiece offers large resistance to cutter tool due to high local stiffness of the thin wall (Joshi and G. Bolar., 2020). The stresses eventually decreases at the end of the machining and lower von- mises stresses could be observed at the end of 0.4 ms.

Fig. 10 shows the main effects plot for stress distribution in the thin wall. As the number of flutes increases, the stress in the thin wall increases. This result is in agreement with the results of jiang et al, that the residual stress increases with increase in the number of cutting teethes according to their proposed mathematical model (Joshi and G. Bolar., 2021). The stresses in the thin wall initially decreased as the helix angle increased from 30^0 to 35^0 but stresses increased for change in helix angle from 35^0 to 45^0. An increase in helix angle results in a significant decrease in the radial cutting force component and thus the resultant cutting force (Li et al 2021). These milling forces induce residual compressive and tensile stresses which decreases with a decrease in the cutting force (Tehranizadeh and Budak, 2017). Hence a decreasing trend was observed in the residual stresses with an increase in the helix angle. The stresses in the thin wall were observed to be minimum when median serration endmill was used and maximum when sinusoidal serration profile endmill was used. The results (Tehranizadeh, 2019), shows that for same cutting conditions, the maximum cutting forces in the trapezoidal serrated endmill was less than the forces observed using circular serration geometry. This reduction in the cutting forces results in the reduction in the stresses in the workpiece during and after machining. Similarly, we have observed lesser stresses in the median serration geometry compared to the sinusoidal serration geometry. The helix angle parameter was the most influential parameter contributing to stress distribution in the thin wall.

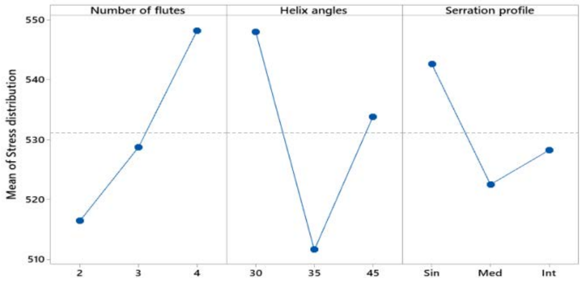

Fig. 10. Main effects plot for stress distribution in the thin wall

ANOVA for stress distribution in thin wall

Table 8 shows the results of ANOVA obtained for the stress distribution in the thin wall. According to the ANOVA, the helix angle parameter has the largest percentage contribution of 47.98 % followed by number of flutes at 37.33 % and serration profile at 14.6 %. The calculated F-value (F_{cal}) for all the three parameters was greater than the critical F-value ($F_{0.05,\ 2,\ 2}$) with 95 % confidence level, hence all three factors have a significant influence on the stress distribution in the thin wall.

Table 8 ANOVA for Stress distribution in the thin wall

Source	DoF	Seq SS	Contribution (%)	Adj MS	p-value	F_{cal}	$F_{0.05}$
Number of flutes	2	1487.33	37.33	743.664	0.003	378.41	19
Helix angle	2	1911.82	47.98	955.911	0.002	486.41	19
Serration geometry	2	581.71	14.60	290.856	0.007	148	19
Error	2	3.93	0.10	1.965			
Total	8	3984.79	100				

Grey relational analysis

Grey relational analysis is an optimization technique based on grey system theory. This method is used to optimize the control factors having multiple responses by assigning certain grades (Girish et al. 2019). While Taguchi method is used to optimize the single response problems, GRA method is used for multi response optimization (Jeyaprakash et al. 2020). The reduction in the deflection and stress in the thin wall induced during machining operations can lead to improved product quality in terms of reduction in surface form errors and improvement in the machining productivity due to decrease in the additional machining requirements. Hence it is desirable to have as minimum amount of deflection and stress in the thin-walled components during and post machining. Hence, “Smaller the better” was selected as the desirable quality characteristic for the performance parameters such as deflection and stresses induced in the thin wall during the grey relational analysis. The numerical results of the performance parameters were normalized using Equation (2) (Zuo et al. 2020).

$$x_i(k)' = \frac{x_i(k) - \min x_i(k)}{\max x_i(k) - \min x_i(k)} \qquad (2)$$

Where $x_i(k)'$ is the normalized data of tabulated SN ratios, $x_i(k)$ is the k[th] response of the i[th] experiment, $\max x_i\,(k)$ is the largest value of $x_i(k)$ for the k[th] response and $\min x_i\,(k)$ is the smallest value of $x_i(k)$ for the k[th] response. The grey relational coefficient (GRC) was calculated for the normalized values using Equation (3) (Manjunatha C et.al 2020).

$$\xi_i(k) = \frac{\Delta_{\min} + l\Delta_{\max}}{\Delta(k) + l\Delta_{\max}} \qquad (3)$$

Where $\xi_i(k)$ is the grey relational coefficient for the i[th] experiment for the k[th] response, l is the resolution coefficient whose value is defined between the range 0 to 1 and in general, l=0.5. $\Delta(k) = |x_o(k) - x_i(k)'|$, $\Delta_{max} = max|x_o(k) - x_i(k)'|$, $\Delta_{min} = min|x_o(k) - x_i(k)'|$, $x_o(k)$ is the reference sequence and $x_i(k)$ is the comparison sequence.

The grey relational grade (GRG) $\bar{\xi_j}$ is calculated using (Jena et.al 2019) the Equation (4). Table 9 predicts the grey relational coefficients and grey relational grades.

$$\bar{\xi_j} = \frac{1}{k}\sum_{i=1}^{m} \xi_{ij} \quad (4)$$

Where $\bar{\xi_j}$ is the grey relational grade for the jth experiment.

Grey relational analysis showed that 4 flutes, 45^0 helix angle and median serration geometry were the optimal process parameters and resulted in grey relational grade of 0.703.

Table 9. Grey relational coefficients and grey relational grade for the responses

Run No.	Normalized values		Grey relational coefficient		Grey relational grade	Rank
	Deflection (mm)	Stress distribution (MPa)	Deflection (mm)	Stress distribution (MPa)		
1	0.000	0.236	0.333	0.395	0.364	9
2	0.247	1.000	0.399	1.000	0.699	2
3	0.644	0.597	0.584	0.554	0.569	4
4	0.692	0.317	0.619	0.423	0.521	6
5	0.631	0.757	0.576	0.673	0.624	3
6	0.554	0.260	0.529	0.403	0.466	8
7	0.840	0.000	0.757	0.333	0.545	5
8	0.705	0.273	0.629	0.408	0.518	7
9	1.000	0.270	1.000	0.407	0.703	1

Table 10 shows the main effects of mean of grey relational grades for each level of factors. The optimal levels of process parameters were obtained at 4 flutes, 35^0 helix angle and median serration geometry which corresponded to maximum grey relational grade at each column of Table 10.

Table 10. Main effects of grey relational grades

Level	No of Flutes	Helix angle	Serration Geometry
1	0.544	0.477	0.450
2	0.537	**0.614**	**0.641**
3	**0.589**	0.579	0.580
Delta	0.052	0.137	0.192
Rank	3	2	1

Validation of the Simulation results

The simulation results obtained for serrated end mills were compared with experimental data available in the open literature as shown in Table 11.

Table 11. Validation of the Simulation results obtained for serrated end mills

References	End mill parameters	Material	Observations
Majed Masmali, Philip Mathew	The milling cutter is 10 mm in diameter, four fluted with a 30° helix angle and 50° helix angle, Cutting Conditions; speed: 50 m/min, feed: 0.04 mm/tooth, width: 0.50 mm, depth: 10 mm	Al 6061 alloy and 0.2% C plain carbon steel	The peak displacement of 0.00783 mm was observed.
Bolar, Gururaj Joshi, Shrikrishna	The cutting tool used was ‘Flat end mill’. The diameters of the end mills was 8mm with 4 flutes and 45o helix angle. The machining condition were 4500 r/min spindle speed, 0.1 mm/tooth feed, 1 mm radial depth of cut and 25 mm axial depth of cut.	Aluminum alloy 2024-T351 with thin wall thickness of 2.5 mm.	The maximum deflection of 0.13 mm was observed in the ends of the thin wall and the maximum induced stress in the machined area was found to be 700 MPa.
Lukic Dejan	An 8 mm diameter end mill with 30o helix angle, 2 flutes and with corner radius 0.6 mm was used for machining 70mm x 40 mm x 40 mm prismatic workpiece into thin wall of thicknesses of 0.5mm, 1 mm and 1.5 mm.	Aluminum alloy 7075	Maximum wall thickness deviation of 0.042 mm, 0.06mm and 0.066 mm were observed when the thin wall thickness changed from 0.5mm, 1mm and 1.5 mm respectively.
Huang et.al	A three-fluted tungsten steel flat end-mill of 10 mm diameter and helix angle 45◦ was used to reduce the thin wall thickness from 2 mm to 0.8 mm with 1500 r/min speed and 360 mm/min feed rate in wet condition.	Aluminum alloy 6061	The maximum wall thickness error (wall deflection) is 0.1227 mm.
Present Research	4 flutes, 45° helix angle and median serration geometry Tungsten carbide serrated endmill.	Aluminium alloy 2024	The maximum deflection observed in the thin wall was 1.032 mm and stress distribution in the thin wall was 561.56 MPa.

CONCLUSIONS

The present paper aimed at analyzing deformation and stresses induced during simulation of thin wall machining using serrated end mill tool. The maximum deflection was obtained when minimum number of flutes, minimum helix angle and sinusoidal serration were adopted. Similarly, minimum deflection was obtained at maximum number of flutes, maximum helix angle and median serration geometry. The stresses in the thin wall got minimized when minimum number of flutes, intermediate helix angle, and median serration geometry were adopted. While the number of flutes significantly affected the thin wall deflection, the helix angle significantly influenced the failure stresses. According to grey relational analysis, the thin wall deflection and stresses could be simultaneously minimized when maximum number of flutes, intermediate helix angle and median serration geometry was adopted.

ACKNOWLEDGMENT

The authors are grateful to management of Rashtreeya Sikshana Samithi Trust (RSST) and Principal, RV College of Engineering, Bengaluru for constant support and encouragement.

REFERENCES

A. C. Okafor and A. A. Sultan, "Development of a mechanistic cutting force model for wavy-edge bull-nose helical end-milling of inconel 718 under emulsion cooling strategy," Applied Mathematical Modelling, vol. 40, no. 4, pp. 2637-2660, (2016).

Bolar, Gururaj, Joshi, Shrikrishna., "Three-dimensional numerical modeling, simulation and experimental validation of milling of a thin-wall component", Proceedings of the Institution of Mechanical Engineers, Part B: Journal of Engineering Manufacture. vol 231, no 5, pp 792-804 (2017)

B. M. Girish, H. S. Siddesh, and B. M. Satish, "Taguchi grey relational analysis for parametric optimization of severe plastic deformation process," SN Applied Sciences, vol. 1, no. 8, pp 937-948, (2019).

F. Tehranizadeh and E. Budak, "Design of Serrated End Mills for Improved Productivity," Procedia CIRP, vol. 58, pp. 493-498, (2017).

F. Tehranizadeh, R. Koca, and E. Budak, "Investigating effects of serration geometry on milling forces and chatter stability for their optimal selection," International Journal of Machine Tools and Manufacture, vol. 144, 103425, (2019).

G. Wu, G. Li, W. Pan, X. Wang, and S. Ding, "A prediction model for the milling of thin-wall parts considering thermal-mechanical coupling and tool wear," International Journal of Advanced Manufacturing Technology, vol. 107, no. 11–12, pp. 4645–4659, (2020).

Huang, Wei-Wei, Zhang, Yang & Zhang, Xin-Quan & Zhu, Li-Min., "Wall thickness error prediction and compensation in end milling of thin-plate parts", Precision Engineering, 66. 550-563. (2020).

J. Burek, M. Plodzien, L. Zylka, and P. Sulkowicz, "High-performance end milling of aluminum alloy: Influence of different serrated cutting edge tool shapes on the cutting force" Advances in Production Engineering and Management, vol. 14, no. 4, pp. 494–506, (2019).

J. K. Rai and P. Xirouchakis, "FEM-based prediction of workpiece transient temperature distribution and deformations during milling," International Journal of Advanced Manufacturing Technology, vol. 42, no. pp 5–12, (2009).

Jena M, Manjunatha, C, Shivaraj B.W, Ashoka S, Sham Aan M.P, "Optimization of parameters for maximizing photocatalytic behaviour of Zn 1-x Fe x O nanoparticles for methyl orange degradation using Taguchi and Grey relational analysis Approach, Materials Today Chemistry, vol 12, pp. 187–199, (2019).

L. Gang, "Study on deformation of titanium thin-walled part in milling process," Journal of Materials Processing Technology, vol. 209, no. 6, pp. 2788-2793, (2009).

L. Junbai and Z. Kai, "Multi-point location theory, method, and application for flexible tooling system in aircraft manufacturing," International Journal of Advanced Manufacturing Technology, vol. 54, no. 5–8, pp. 729-736, (2011).

Lukic, Dejan, Cep, Robert,Vukman, Jovan Antic, Aco, Durdev, Mica, Milosevic, Mijodrag., "Multi-Criteria Selection of the Optimal Parameters for High-Speed Machining of Aluminum Alloy Al7075 Thin-Walled Parts". Metals. vol 10, no12, 1570-1578. (2020).

Majed Masmali, Philip Mathew, "An Analytical Approach for Machining Thin-walled Workpieces", Procedia CIRP, vol. 58, pp 187-192 (2017).

Manjunatha C, Abhishek B, Shivaraj B.W, Shashank M, Nagaraju G, "Engineering the MxZn1−xO (M= Al3+,Fe3+,Cr3+) nanoparticles for visible light-assisted catalytic mineralization of methylene blue dye using Taguchi design", Journal of chemical papers, vol 74, no 8, pp. 2719–2731, (2020).

M. Li, J. Huang, W. Ding, X. Liu, and L. Li, "Dynamic response analysis of a ball-end milling cutter and optimization of the machining parameters for a ruled surface," Proceedings of the Institution of Mechanical Engineers, Part B: Journal of Engineering Manufacture, vol. 233, no. 2, pp. 588-599, (2019).

Naveed Iqbal Ansari, P Sivagnanapalani, V Sureshkumar, BW Shivaraj, PK Panda, "Synthesis of lanthanum titanate (La2Ti2O7) for high temperature sensor applications", Journal of Materials Science: Materials in Electronics, Vol 32,no 23, pp 27422-27428 (2021)

N. Jeyaprakash, C. H. Yang, and D. Raj Kumar, "Machinability study on CFRP composite using Taguchi based grey relational analysis," Materials Today: Proceedings, vol. 21, pp. 1425-1431, (2020).

P. Kersting and D. Biermann, "Modeling techniques for simulating workpiece deflections in NC milling," CIRP Journal of Manufacturing Science and Technology, vol. 7, no.1, pp. 48–54, (2014).

P. Bari, M. Law, and P. Wahi, "Improved chip thickness model for serrated end milling," CIRP Journal of Manufacturing Science and Technology, vol. 25, pp. 36-49, (2019).

P. Bari, M. Law, and P. Wahi, "Investigations on the Influence of Radial Run-Out on Cutting Forces for Serrated Cutters," Proceedings of the 2nd International Conference on Advances in Computational Methods in Manufacturing, pp. 1-10, (2019).

R. Izamshah, M. Y. Yuhazri, M. Hadzley, M. Amran, and S. Subramonian, "Effects of end mill helix angle on accuracy for machining Thin-Rib Aerospace Components," Applied Mechanics and Materials, vol. 315, pp. 773-777, (2013).

R. Koca and E. Budak, "Optimization of serrated end mills for reduced cutting energy and higher stability," in Procedia CIRP, vol. 8, pp. 570-575, (2013).

P. Bari, P. Wahi, and M. Law, "Investigations on the Influence of Serration Parameters on Cutting Forces," vol 15, pp 189-204, (2019).

S Herranz, F J Campa, L N Lopez de Lacalle, A Rivero, A Lamikiz, E Ukar, J A Sanchez, U Bravo, "The milling of airframe components with low rigidity: A general approach to avoid static and dynamic problems," Journal of Engineering Manufacture, vol. 219, no. 11, pp. 789–801, (2005).

S. Li, J. Sui, F. Ding, S. Wu, W. Chen, and C. Wang, "Optimization of Milling Aluminum Alloy 6061-T6 using Modified Johnson-Cook Model," Simulation Modelling Practice and Theory, vol. 111,pp 102330 (2021).

S. N. Joshi and G. Bolar, "Three-Dimensional Finite Element Based Numerical Simulation of Machining of Thin-Wall Components with Varying Wall Constraints," Journal of The Institution of Engineers (India): Series C, vol. 98, no. 3, pp. 343-352, (2017).

S. N. Joshi and G. Bolar, "Influence of End Mill Geometry on Milling Force and Surface Integrity While Machining Low Rigidity Parts," Journal of The Institution of Engineers (India): Series C, 102,1503-1511, (2021).

S. Zeng, X. Wan, W. Li, Z. Yin, and Y. Xiong, "A novel approach to fixture design on suppressing machining vibration of flexible workpiece," International Journal of Machine Tools and Manufacture, vol. 58, pp. 29-43, (2012).

T. Aijun and L. Zhanqiang, "Deformations of thin-walled plate due to static end milling force," Journal of Materials Processing Technology, vol. 206, no. 1–3, pp. 345-351, (2008).

W. Chen, J. Xue, D. Tang, H. Chen, and S. Qu, "Deformation prediction and error compensation in multilayer milling processes for thin-walled parts," International Journal of Machine Tools and Manufacture, vol. 49, no. 11,pp 859-864, (2009).

W. Zuo, J. Li, Y. Zhang, Q. Li, and Z. He, "Effects of multi-factors on comprehensive performance of a hydrogen-fueled micro-cylindrical combustor by combining grey relational analysis and analysis of variance," Energy, vol. 199, 11439, (2020).

X. Jiang, B. Li, J. Yang, and X. Y. Zuo, "Effects of tool diameters on the residual stress and distortion induced by milling of thin-walled part," International Journal of Advanced Manufacturing Technology, vol. 68, no. 1–4, pp 175-186,(2013).

X. J. Wan, L. Hua, X. F. Wang, Q. Z. Peng, and X. P. Qin, "An error control approach to tool path adjustment conforming to the deformation of thin-walled workpiece," International Journal of Machine Tools and Manufacture, vol. 51, no. 3, pp. 221-229, (2011).

X. Jiang, X. Kong, Z. Zhang, Z. Wu, Z. Ding, and M. Guo, "Modeling the effects of Undeformed Chip Volume (UCV) on residual stresses during the milling of curved thin-walled parts," International Journal of Mechanical Sciences, vol. 167,105162 (2020).

X. Jiang, Y. Zhu, Z. Zhang, M. Guo, and Z. Ding, "Investigation of residual impact stress and its effects on the precision during milling of the thin-walled part," International Journal of Advanced Manufacturing Technology, vol. 97, no 2. pp 1–4, (2018).

Y. Guo, B. Lin, and W. Wang, "Modeling of cutting forces with a serrated end mill," Mathematical Problems in Engineering, vol 1, pp 1-13, (2019).

Z. Dombovari, Y. Altintas, and G. Stepan, "The effect of serration on mechanics and stability of milling cutters," International Journal of Machine Tools and Manufacture, vol. 50, no. 6, pp. 511-520, (2010).